Published in final edited form as:

Nature. 2016 October 13; 538(7624): 270–273. doi:10.1038/nature19802.

Two Distinct RNase Activities of CRISPR-C2c2 Enable Guide RNA Processing and RNA Detection

Alexandra East-Seletsky[1,*], **Mitchell R. O'Connell**[1,*], **Spencer C. Knight**[2], **David Burstein**[3], **Jamie H. D. Cate**[1,2,8], **Robert Tjian**[1,4,5,6], and **Jennifer A. Doudna**[1,2,5,7,8]

[1]Department of Molecular and Cell Biology, University of California, Berkeley, California, 94720, USA

[2]Department of Chemistry, University of California, Berkeley, California, 94720, USA

[3]Department of Earth And Planetary Sciences, University of California, Berkeley, California, 94720, USA

[4]Janelia Research Campus, Howard Hughes Medical Institute, Ashburn, VA, USA

[5]Howard Hughes Medical Institute, University of California, Berkeley, California 94720, USA

[6]Li Ka Shing Biomedical and Health Sciences Center, University of California, Berkeley, CA, USA

[7]Innovative Genomics Initiative, University of California, Berkeley, California 94720, USA

[8]MBIB Division, Lawrence Berkeley National Laboratory, Berkeley, California 94720, USA

Abstract

Bacterial adaptive immune systems employ CRISPRs (clustered regularly interspaced short palindromic repeats) and CRISPR-associated (Cas) proteins for RNA-guided nucleic acid cleavage[1,2]. Although generally targeted to DNA substrates[3–5], the Type III and Type VI CRISPR systems direct interference complexes against single-stranded RNA (ssRNA) substrates[6–9]. In Type VI systems, the single-subunit C2c2 protein functions as an RNA-guided RNA endonuclease[9,10]. How this enzyme acquires mature CRISPR RNAs (crRNAs) essential for immune surveillance and its mechanism of crRNA-mediated RNA cleavage remain unclear. Here we show that C2c2 possesses a unique ribonuclease activity responsible for CRISPR RNA maturation that is distinct from its RNA-activated ssRNA-degradation activity. These dual ribonuclease functions are chemically and mechanistically different from each other and from the crRNA-processing behavior of the evolutionarily unrelated CRISPR enzyme Cpf1[11]. We show that

Correspondence and requests for materials should be addressed to J.A.D. (doudna@berkeley.edu).
*These authors contributed equally to this work.

ONLINE CONTENT

Methods, along with additional Extended Data display items, Supplementary Files, and Source Data, are available in the online version of the paper; references unique to these sections appear only in the online paper.

AUTHOR CONTRIBUTIONS

A.E.S., M.R.O., S.C.K. conceived the study and designed experiments with input from J.H.D.C., R.T. and J.A.D. D.B. performed bioinformatic analyses. A.E.S. and M.R.O. executed all experimental work with assistance from S.C.K. All authors discussed the data and wrote the manuscript.

The authors are inventors on a related patent application.

the two ribonuclease activities of C2c2 enable multiplexed processing and loading of guide RNAs that in turn allow for sensitive cellular transcript detection.

The essential first step of CRISPR immune surveillance requires processing of precursor crRNA transcripts (pre-crRNAs), consisting of repeat sequences flanking viral spacer sequences, into individual mature crRNAs that each contain a single spacer[12–14]. CRISPR systems employ three known mechanisms to produce mature crRNAs: a dedicated endonuclease (e.g., Cas6 or Cas5d in Type I and III systems) [15–17], coupling of a host endonuclease (e.g., RNase III with a trans-activating crRNA (tracrRNA) in Type II systems)[18], or a ribonuclease activity intrinsic to the effector enzyme itself (e.g., Cpf1, Type V systems) [11].

Since Type VI CRISPR loci lack an obvious Cas6 or Cas5d-like endonuclease or tracrRNA[10], we wondered whether C2c2 itself might possess pre-crRNA processing activity, and if so, whether the mechanism would be distinct from Cpf1, an unrelated class 2 CRISPR effector recently demonstrated to process pre-crRNAs[11]. Using purified recombinant C2c2 protein homologs from three distinct branches of the C2c2 protein family (Fig. 1a–b and Extended Data Figs. 1–2), we found that all three C2c2 enzymes cleave 5′-end radiolabeled pre-crRNA substrates consisting of a full-length consensus repeat sequence and a 20 nucleotide (nt) spacer sequence (Fig. 1c). We mapped the cleavage site for each pre-crRNA:C2c2 homolog pair, revealing that processing occurs at a position either two or five nucleotides upstream of the predicted repeat-sequence hairpin structure, depending on the C2c2 homolog (Fig. 1c, Extended Data Fig. 3a). Surprisingly, our biochemically mapped 5′-cleavage sites do not agree with previously reported cleavage sites for *Leptotrichia shahii* (LshC2c2) or *Listeria seeligeri* (LseC2c2) pre-crRNAs[10]. Our own analysis of Shmakov *et al.*'s RNA sequencing data set indicates agreement of the *in vivo* cleavage site with the *in vitro* site reported here (Extended Data Fig. 3b–i). Furthermore, cleavage assays using C2c2 from *Leptotricia buccalis* (LbuC2c2) and a larger pre-crRNA comprising a tandem hairpin-repeat array resulted in two products resulting from two separate cleavage events (Extended Data Fig. 4a), consistent with a role for C2c2 in processing precursor crRNA transcripts generated from Type VI CRISPR loci.

To understand the substrate requirements and mechanism of C2c2 guide RNA processing, we generated pre-crRNAs harboring mutations in either the stem loop or the single-stranded flanking regions of the consensus repeat sequence and tested their ability to be processed by LbuC2c2 (Fig. 2). We found that C2c2-catalyzed cleavage was attenuated upon altering the length of the stem in the repeat region (Fig. 2a). Inversion of the stem loop or reduction of the loop length also reduced C2c2's processing activity, while contiguous 4-nt mutations including or near the scissile bond completely abolished it (Extended Data Fig. 7b). A more extensive mutational analysis of the full crRNA repeat sequence revealed two distinct regions on either side of the hairpin with marked sensitivity to base changes (Fig. 2b). By contrast, there was no dependence on the spacer sequence for kinetics of processing (Extended Data Fig. 4c). This sensitivity to both flanking regions of the hairpin is reminiscent of the sequence and structural motifs required by many Cas6 and Cas5d

enzymes[12,13,19]. In contrast, Cpf1 does not have any dependence on the 3′ hairpin flanking region, as the variable spacer region abuts the hairpin stem[11].

Mechanistic studies of LbuC2c2 revealed that processing activity was unaffected by the presence of divalent metal ion chelators EDTA or EGTA (Fig. 2c), indicative of a metal ion-independent RNA hydrolytic mechanism. Metal ion-independent RNA hydrolysis is typified by the formation of a 2′, 3′-cyclic phosphate and 5′-hydroxide on the 5′ and 3′ halves of the crRNA cleavage products, respectively[20]. To determine the end-group chemical identity of C2c2-processed substrates, we further incubated the 5′ flanking products with T4 polynucleotide kinase, which removes 2′,3′-cyclic phosphates to leave a 3′-hydroxyl. We observed altered denaturing-gel migration of the 5′ flanking product after kinase treatment, consistent with the removal of a 3′ phosphate group (Extended Data Fig. 4d). The divalent metal ion independence of C2c2's pre-crRNA processing activity is in stark contrast with the divalent metal ion dependency of Cpf1, the only other single-protein CRISPR effector shown to perform guide processing[11]. Collectively, these data indicate that C2c2-catalyzed pre-crRNA cleavage is a divalent metal ion-independent process that likely uses a general acid-base catalysis mechanism[20].

Following maturation, crRNAs typically bind with high affinity to Cas effector protein(s) to create RNA-guided surveillance complexes capable of sequence-specific nucleic acid recognition[1,2,21]. In agreement with previous work using LshC2c2[9], LbuC2c2 catalyzed efficient target RNA cleavage only when such substrates could base pair with a complementary sequence in the crRNA (Extended Data Figs. 5–7). Given the promiscuous pattern of cleavage observed for C2c2 (Extended Data Fig. 6), we tested the ability of LbuC2c2 to act as a crRNA-activated non-specific RNA endonuclease in *trans* (Extended Data Fig. 5b). In striking contrast to non-target cleavage experiments performed in *cis* and consistent with observations for LshC2c2[9], we observed rapid degradation of non-target RNA in *trans* (Extended Data Fig. 5b). This result shows that target recognition activates C2c2 for general non-specific degradation of RNA. Importantly, the similar RNA cleavage rates and near-identical cleavage products observed for both *cis* on-target cleavage and *trans* non-target cleavage of the same RNA substrate implicate the same nuclease center in both activities (Extended Data Fig. 5b).

Notably, crRNA-mediated cleavage of target ssRNA occurs at an ~80-fold faster rate than pre-crRNA processing (Fig. 3a), and in contrast to pre-crRNA processing, RNA-guided target cleavage is abolished in the presence of EDTA, indicating that this activity is divalent metal ion-dependent (Fig. 3a, (Extended Data Fig. 5c, Extended Data Fig. 7). Given these clear differences, we reasoned that C2c2 might possess two orthogonal RNA cleavage activities: one for crRNA maturation, and the other for crRNA-directed, non-specific RNA degradation. To test this hypothesis, we systematically mutated several residues within the conserved HEPN motifs of LbuC2c2[9,22–24], and assessed pre-crRNA processing and RNA-guided RNase activity of the mutants (Fig. 3, Extended Data Fig. 7d). Double and quadruple mutants of conserved HEPN residues (R472A, R477A, R1048A and R1053) retained robust pre-crRNA cleavage activity (Fig. 3c). By contrast, all HEPN mutations abolished RNA-guided cleavage activity while not affecting crRNA or ssRNA-binding ability (Extended Data Fig. 7d, 8)[9].

Next we sought mutations that would abrogate pre-crRNA processing activity without disrupting target RNA cleavage. Given that we were unable to predict any other potential RNase motifs beyond the HEPN motifs, and that C2c2 proteins bear no homology to Cpf1, we opted to systematically mutate the charged residues throughout LbuC2c2. We identified an arginine residue (R1079A) that upon mutation resulted in severely attenuated pre-crRNA processing activity (Fig. 3c). This C2c2 mutant enzyme retained crRNA-binding ability as well as RNA target cleavage activity (Extended Data Fig. 8d, Fig. 3d,). Taken together, our results show that distinct active sites within the C2c2 protein catalyze pre-crRNA processing and RNA-directed RNA cleavage.

We recognized that C2c2's robust RNA-stimulated cleavage of *trans* substrates might be employed as a means of detecting specific RNAs within a pool of transcripts. While many polymerase-based methods have been developed for RNA amplification and subsequent detection, few approaches are able to directly detect the target RNA without significant engineering or stringent design constraints for each new RNA target[20,25–27]. As a readily-programmable alternative, we tested whether C2c2's RNA-guided *trans* endonuclease activity could be harnessed to cleave a fluorophore-quencher-labeled reporter RNA substrate, thereby resulting in increased fluorescence upon target RNA-triggered RNase activation (Fig. 4a). LbuC2c2 was loaded with bacteriophage λ-targeting crRNAs and tested for its ability to detect the corresponding λ ssRNA targets spiked into HeLa cell total RNA. We found that upon addition of as little as 1–10 pM complementary λ target-RNA, a substantial crRNA-specific increase in fluorescence occurred within 30 min (Fig. 4b and Extended Data Fig. 9a). Control experiments with either C2c2:crRNA complex alone or in the presence of crRNA and a non-complementary target RNA resulted in negligible increases in fluorescence relative to an RNase A positive control (Fig. 4b and Extended Data Fig. 9a). We note that at the 10 pM concentration of a λ target RNA, only ~0.02% of the C2c2:crRNA complex is predicted to be in the active state, yet the observed fluorescent signal reflected ~25–50% cleavage of the reporter RNA substrate, depending on the RNA target. Fragment size resolution of the background RNA in these reactions revealed significant degradation, even on highly structured tRNAs (Extended Data Fig. 9b). Since reporter RNA cleavage occurs in the presence of a vast excess of unlabeled RNA, we conclude that LbuC2c2 is a robust multiple-turnover enzyme capable of at least 10^4 turnovers per target RNA recognized. Thus, in contrast to previous observations[9], crRNA-directed *trans* cleavage is potent and detectable even at extremely low levels of activated protein.

To extend this LbuC2c2 RNA detection system, we designed a crRNA to target endogenous beta-actin mRNA. We observed a measurable increase in fluorescence in the presence of human total RNA relative to *E. coli* total RNA, demonstrating the specificity of this method (Fig. 4c). Furthermore, given that C2c2 processes its own guide, we combined pre-crRNA processing and RNA detection in a single reaction by designing tandem crRNA-repeat containing spacers complementary to target RNAs A and λ2. LbuC2c2 incubated with this unprocessed tandem guide RNA in the detection assay generated a significant increase in fluorescence similar in magnitude and sensitivity to experiments using mature crRNAs (Fig. 4b, d). Taken together, these data highlight the exciting opportunity to take advantage of C2c2's two distinct RNase activities for a range of biotechnological applications (Fig. 4e).

In bacteria, C2c2 likely operates as a sentinel for viral RNAs[9]. We propose that when invasive transcripts are detected within the host cell via base pairing with crRNAs, C2c2 is activated for promiscuous cleavage of RNA in *trans* (Fig. 4e). As a defense mechanism, this bears striking similarity to RNase L and caspase systems in eukaryotes, whereby a cellular signal triggers promiscuous ribonucleolytic or proteolytic degradation within the host cell, respectively, leading to apoptosis[28,29]. While the RNA targeting mechanisms of Type III CRISPR systems generally result in RNA cleavage within the protospacer-guide duplex[8,30], recent examples of associated nucleases Csx1[23] and Csm6[24] provide compelling parallels between the Type VI systems and the multi-component Type III inference complexes.

Our data show that CRISPR-C2c2 proteins represent a new class of enzyme capable of two separate RNA recognition and cleavage activities. Efficient pre-crRNA processing requires sequence and structural motifs within the CRISPR repeat which prevent non-endogenous crRNA loading and helps to reduce the potential toxicity of this potent RNase. The entirely different pre-crRNA processing mechanisms of C2c2 and the Type V CRISPR effector protein Cpf1 indicate that each protein family has converged upon independent activities encompassing both the processing and interference functions of their respective CRISPR pathways. Furthermore, the two distinct catalytic capabilities of C2c2 can be harnessed in concert for RNA detection, as the activation of C2c2 to cleave thousands of *trans*-RNAs for every target RNA detected enables potent signal amplification. The capacity of C2c2 to process its own guide RNAs from arrays could also allow the use of tissue-specific Pol II promoters for guide expression, in addition to target multiplexing for a wide range of applications. The C2c2 enzyme is unique within bacterial adaptive immunity for its dual RNase activities, and highlights the utility of harnessing CRISPR proteins for precise nucleic acid manipulation in cells and cell-free systems.

METHODS

C2c2 phylogenic and candidate selection

C2c2 maximum-likelihood phylogenies were computed using RAxML[31] with the PROTGAMMALG evolutionary model and 100 bootstrap samplings. Sequences were aligned by MAFFT with the ‘einsi’ method[32].

C2c2 protein production and purification

Expression vectors for protein purification were assembled using synthenic gBlocks ordered from Integrated DNA Technologies. The codon-optimized C2c2 genomic sequence was *N*-terminally tagged with a His_6-MBP-TEV cleavage site, with expression driven by a T7 promoter. Mutant proteins were cloned via site-directed mutagenesis of wild-type C2c2 constructs. Expression vectors were transformed into Rosetta2 *E. coli* cells grown in 2xYT broth at 37 °C. *E. coli* cells were induced during log phase with 0.5 M ITPG, and the temperature was reduced to 16 °C for overnight expression of His-MBP-C2c2. Cells were subsequently harvested, resuspended in lysis buffer (50 mM Tris-HCl pH 7.0, 500 mM NaCl, 5% glycerol, 1 mM TCEP, 0.5mM PMSF, and EDTA-free protease inhibitor (Roche)) and lysed by sonication, and the lysates were clarified by centrifugation. Soluble His-MBP-C2c2 was isolated over metal ion affinity chromatography, and protein-containing eluate was

incubated with TEV protease at 4 °C overnight while dialyzing into ion exchange buffer (50 mM Tris-HCl pH 7.0, 250 mM KCl, 5% glycerol, 1 mM TCEP) in order to cleave off the His_6-MBP tag. Cleaved protein was loaded onto a HiTrap SP column and eluted over a linear KCl (0.25–1.5M) gradient. Cation exchange chromatography fractions were pooled and concentrated with 30 kD cutoff concentrators (Thermo Fisher). The C2c2 protein was further purified via size-exclusion chromatography on an S200 column and stored in gel filtration buffer (20 mM Tris-HCl pH 7.0, 200 mM KCl, 5% glycerol, 1 mM TCEP) for subsequent enzymatic assays. Expression plasmids are deposited with Addgene.

Generation of RNA

All RNAs used in this study were transcribed *in vitro* except for crRNA AES461 which was ordered synthetically (Integrated DNA Technologies) [see Extended Data Table 1 and Extended Data Fig. 6]. *In vitro* transcription reactions were performed as previously described with the following modifications: the T7 polymerase concentration was reduced to 10 μg/mL, and the UTP concentration was reduced to 2.5 mM[33]. Transcriptions were incubated at 37°C for 1–2 hr to reduce non-template addition of nucleotides and quenched via treatment with DNase I at 37°C for 0.5–1 hr. Transcription reactions were purified by 15% denaturing polyacrylamide gel electrophoresis (PAGE), and all RNAs were resuspended in cleavage buffer (20 mM HEPES pH 6.8, 50 mM KCl, 5 mM $MgCl_2$, and 5% glycerol). For radioactive experiments, 5′ triphosphates were removed by calf intestinal phosphate (New England Biolabs) prior to radiolabeling and ssRNA substrates were then 5′-end labeled using T4 polynucleotide kinase (New England Biolabs) and [γ-32P]-ATP (Perkin Elmer) as described previously33.

Pre-crRNA processing assays

Pre-crRNA cleavage assays were performed at 37 °C in RNA processing buffer (20 mM HEPES pH 6.8, 50 mM KCl, 5 mM $MgCl_2$, 10 μg/mL BSA, 10 μg/mL tRNA, 0.05% Igepal CA-630 and 5% glycerol) with a 100-fold molar excess of C2c2 relative to 5′-labeled pre-crRNA (final concentrations of 100 nM and <1 nM, respectively). Unless otherwise indicated, reaction was quenched after 60 min with 1.5X RNA loading dye (100% formamide, 0.025 w/v% bromophenol blue, and 200 μg mL^{-1} heparin). After quenching, reactions were denatured at 95 °C for 5 min prior to resolving by 12% or 15% denaturing PAGE (0.5X TBE buffer). Metal dependence of the reaction was tested by addition of EDTA or EGTA to reaction buffer at concentrations varying from 10–100 mM. Bands were visualized by phosphorimaging and quantified with ImageQuant (GE Healthcare). The percent cleavage was determined as the ratio of the product band intensity to the total intensity of both the product and uncleaved pre-crRNA bands and normalized for background within each measured substrate using ImageQuant TL Software (GE Healthcare) and fit to a one phase exponential association using Prism (GraphPad).

Product Size Mapping and 3′ end moiety identification

Cleavage product length was determined biochemically by comparing gel migration of product bands to alkaline hydrolysis and RNase T1 digestion ladders using the RNase T1 Kit from Ambion. For hydrolysis ladder, 15 nM full-length RNA substrates were incubated at 95°C in 1X alkaline hydrolysis buffer (Ambion) for 5 min. Reactions were quenched with

1.5X RNA loading buffer, and cooled to −20°C to immediately stop hydrolysis. For RNase T1 ladder, 15 nM full length RNA substrates were unfolded in 1X RNA sequencing buffer (Ambion) at 65°C. Reactions were cooled to ambient temperature, and then 1 U of RNase T1 (Ambion) was added to reaction. After 15 min, reactions were stopped by phenol-chlorofrom extraction and 1.5X RNA loading buffer was added for storage. Hydrolysis bands were resolved in parallel to cleavage samples on 15% denaturing PAGE and visualized by phosphorimaging. For 3′ end moiety identification, products from the processing reaction were incubated with 10 U of T4 polynucleotide kinase (New England Biolabs) for 1 hr at 37°C in processing buffer. Reactions were quenched with 1.5X RNA loading buffer, resolved on 20% denaturing PAGE and visualized by phosphorimaging.

Small RNA sequencing analysis

RNA reads from Smakov *et al.*[10] were downloaded from SRA runs SRR3713697, SRR3713948, and SRR3713950. The paired-end reads were locally mapped to the reference sequences using Bowtie2[34] with the following options: "--reorder --very-fast-local --local". The mapping was then filtered to retain only alignments that contained no mismatch using mapped.py (https://github.com/christophertbrown/mapped) with the "-m 0 -p both" options. BAM file of the resulting mapping are in the supplementary files for this manuscript. Read coverage was visualized using Geneious and plotted using Prism (GraphPad).

Target cleavage assays

Target cleavages assays were performed at 25 °C or 37 °C in cleavage buffer (20 mM HEPES pH 6.8, 50 mM KCl, 5 mM $MgCl_2$, and 5% glycerol). crRNA guides were pre-folded by heating to 65 °C for 5 min and then slowly cooling to ambient temperature in cleavage buffer. C2c2:crRNA complex formation was performed in cleavage buffer, generally at a molar ratio of 2:1 protein to crRNA at 37 °C for 10 min, prior to adding 5′-end labeled target and/or other non-radiolabeled RNA target substrates. Unless otherwise indicated, final concentrations of protein, guide, and targets were 100 nM, 50 nM, and <1 nM respectively for all reactions. Reactions were quenched with 1.5X RNA loading dye and resolved by 15% denaturing PAGE (0.5X TBE buffer). Bands were visualized by phosphorimaging and quantified with ImageQuant (GE Healthcare). The percent cleavage was determined as the ratio of total banding intensity for all shorter products relative to the uncleaved band and normalized for background within each measured substrate using ImageQuant TL Software (GE Healthcare) and fit to a one phase exponential association using Prism (GraphPad).

crRNA filter-binding assays

Filter binding assays was carried out in RNA processing buffer (20 mM HEPES pH 6.8, 50 mM KCl, 5 mM $MgCl_2$, 10 μg/mL BSA, 10 μg/mL yeast tRNA, 0.01% Igepal CA-630 and 5% glycerol). LbuC2c2 was incubated with radiolabeled crRNA (<0.1 nM) for 1hr at 37°C. Tufryn, Protran and Hybond-N+ were assembled onto a dot-blot apparatus in the order listed above. The membranes were washed twice with 50μL Equilibration Buffer (20 mM HEPES pH 6.8, 50 mM KCl, 5 mM $MgCl_2$ and 5% glycerol) before the sample was applied to the membranes. Membranes were again washed with 50 μL Equilibration Buffer, dried and visualized by phosphorimaging. Data were quantified with ImageQuant TL Software (GE

Healthcare) and fit to a binding isotherm using Prism (GraphPad Software). All experiments were carried out in triplicate. Dissociation constants and associated errors are reported in the figure legends.

Electrophoretic mobility-shift assays

In order to avoid the dissociation of the LbuC2c2-dHEPN1/dHEPN2: crRNA complex at low concentrations during ssRNA-binding experiments, binding reactions contained a constant excess of LbuC22c2-dHEPN1/dHEPN2 (200 nM), and increasing concentrations of crRNA-A and < 0.1 nM target ssRNA. Assays were carried out in C2c2 EMSA buffer (20 mM HEPES pH 6.8, 50 mM KCl, 10 μg/mL BSA, 100 μg/mL yeast tRNA, 0.01% Igepal CA-630 and 5% glycerol). LbuC2c2-crRNA-A complexes were pre-formed as described above for 10 min at 37°C before the addition of 5′-radiolabelled ssRNA substrate and a further incubation for 45 min at 37°C. Samples were then resolved by 8% native PAGE at 4°C (0.5X TBE buffer). Gels were imaged by phosphorimaging, quantified using ImageQuant TL Software (GE Healthcare) and fit to a binding isotherm using Prism (GraphPad Software). All experiments were carried out in triplicate. Dissociation constants and associated errors are reported in the figure legends.

Fluorescent RNA detection assay

LbuC2c2:crRNA complexes were preassembled by incubating 1μM of Lbu-C2c2:C2c2 with 500 nM of crRNA for 10 min at 37°C. These complexes were then diluted to 100nM LbuC2c2: 50 nM crRNA-**λ**2 in RNA processing buffer (20 mM HEPES pH 6.8, 50 mM KCl, 5 mM $MgCl_2$, 10 μg/mL BSA, 10 μg/mL yeast tRNA, 0.01% Igepal CA-630 and 5% glycerol) in the presence of 185 nM of RNAase-Alert substrate (Thermo-Fisher), 100 ng of HeLa total RNA and increasing amounts of target 60 nt ssRNA (0–1 nM). These reactions were incubated in a fluorescence plate reader for up to 120 min at 37°C with fluorescence measurements taken every 5 min (λ_{ex}: 485 nm; λ_{em}: 535 nm). Background-corrected fluorescence values were obtained by subtracting fluorescence values obtained from reactions carried out in the absence of target ssRNA. Maximal fluorescence was measured by incubating 50 nM RNaseA with 185 nM of RNAase-Alert substrate. For measurement of crRNA-ACTB mediated LbuC2c2 activation by *beta-actin* mRNA in human total RNA, LbuCas9:crRNA complexes were preassembled by incubating 1μM of LbuC2c2 with 500 nM of crRNA-ACTB for 10 min at 37°C and reactions were carried out in the conditions above in the presence of increasing amounts (0–1 μg) of either HeLa cell total RNA or E. Coli total RNA (as a negative control). These reactions were incubated in a fluorescence plate reader for up to 180 min at 37°C with fluorescence measurements taken every 5 min (λ_{ex}: 485 nm; λ_{em}: 535 nm). Background-corrected fluorescence values were obtained by subtracting fluorescence values obtained from reactions carried out in the absence of target ssRNA. For coupled pre-crRNA processing and RNA detection assays, LbuCas9-crRNA complexes were preassembled by incubating 1μM of LbuC2c2 with 500 nM of pre-crRNA-A-λ2 for 20 min at 37°C and reactions carried out as described above in the presence of increasing amounts of ssRNA A and ssRNA λ2 (0–1 nM each). In each case, error bars represent the standard deviation from three independent experiments.

Background cleavage in total RNA

LbuC2c2:crRNAλ4 complexes were assembled as previously described for fluorescence RNA detection assay. Complexes were incubated in RNA processing buffer in the presence of 3 ug total RNA with and without 10 nM λ4 ssRNA target. After 2 hr, RNA was isolated by trizol extraction and ethanol precipitation. The RNA fragment size distribution of resuspended samples was resolved using Small RNA Analysis Kit (Agilent) on a Bioanalyzer 2100 (Agilent) using the manufacturer's protocol. Fluorescent intensity curves were normalized in Prism for curve overlay (GraphPad Software).

Extended Data

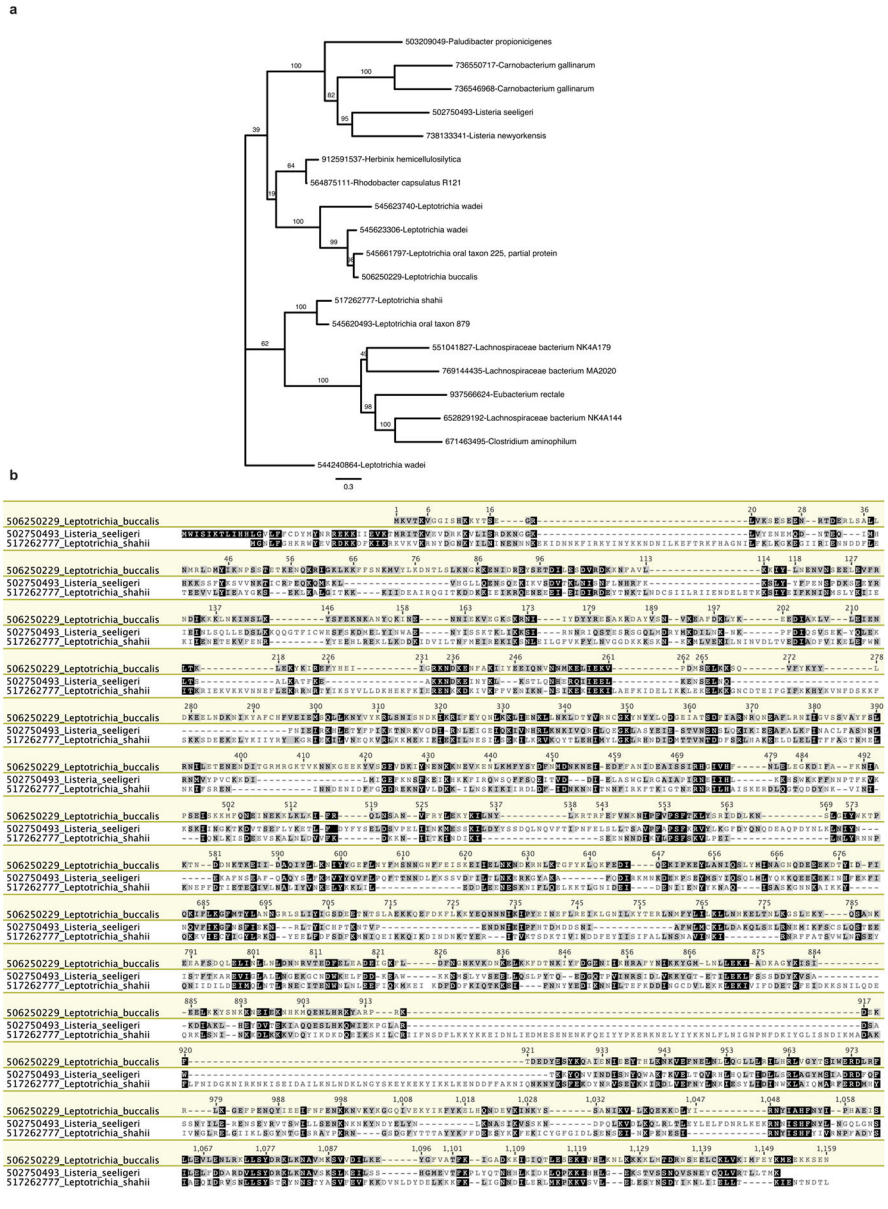

Extended Data Figure 1. Complete phylogenetic tree of C2c2 family and C2c2 alignment

a, Maximum-likelihood phylogenetic reconstuction of C2c2 proteins. Leaves include GI protein numbers and organism of origin; bootstrap support values, out of 100 resamplings, are presented for inner split. Scale is in substitutions per site. **b,** Multiple sequence alignment of the three analyzed homologs of C2c2; coordinates are based on LbuC2c2.

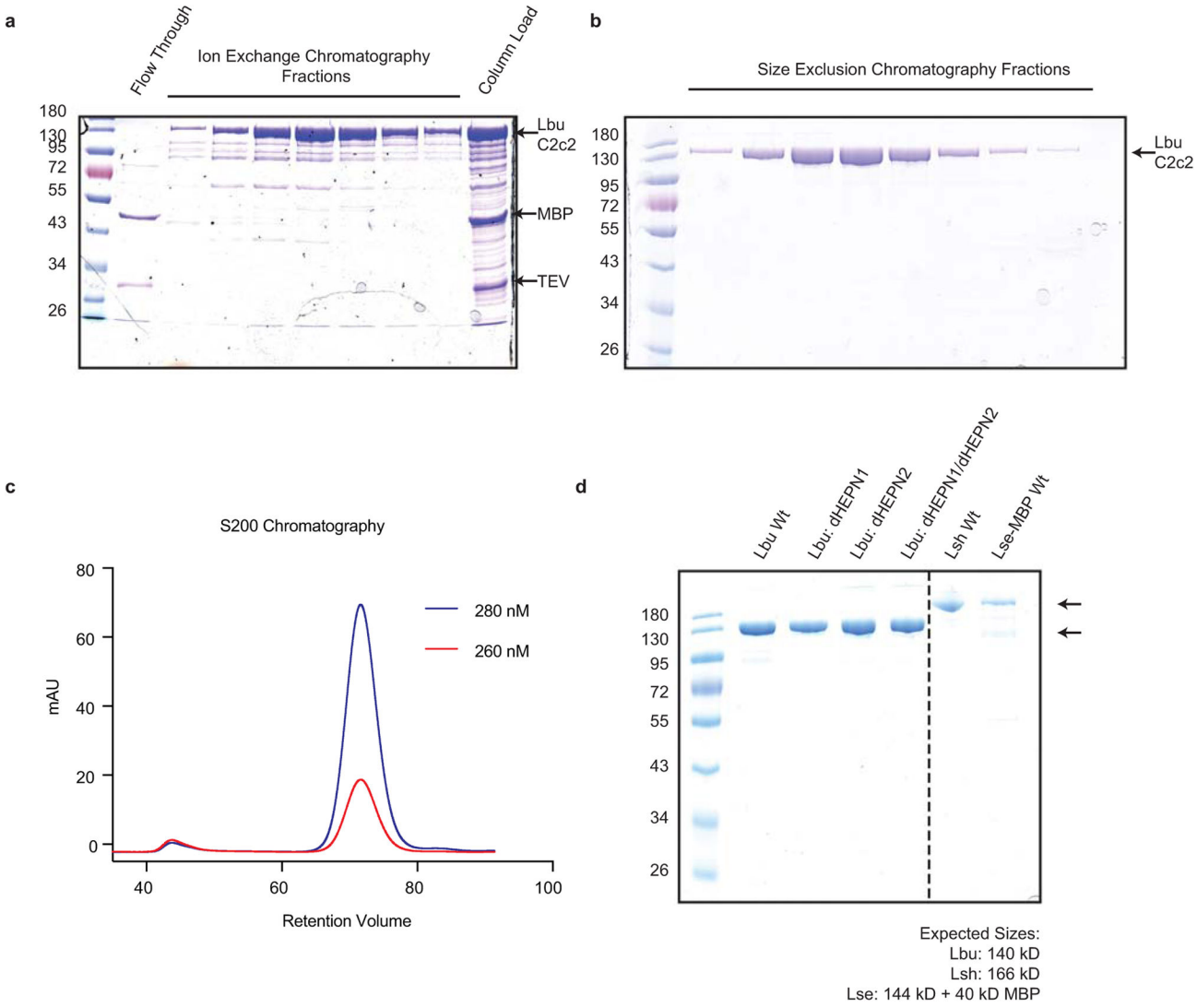

Extended Data Figure 2. Purification and Production of C2c2

All C2c2 homologs were expressed in *E. coli* as His-MBP fusions and purified by a combination of affinity, ion exchange and size exclusion chromatography. The Ni^{+} affinity tag was removed by incubation with TEV protease. Representative SDS-PAGE gels of chromatography fractions are shown in **(a, b). c,** The chromatogram from Superdex 200 (16/60) column demonstrating that C2c2 elutes as a single peak, devoid of nucleic acid. **d,** SDS PAGE analysis of purified proteins used in this manuscript.

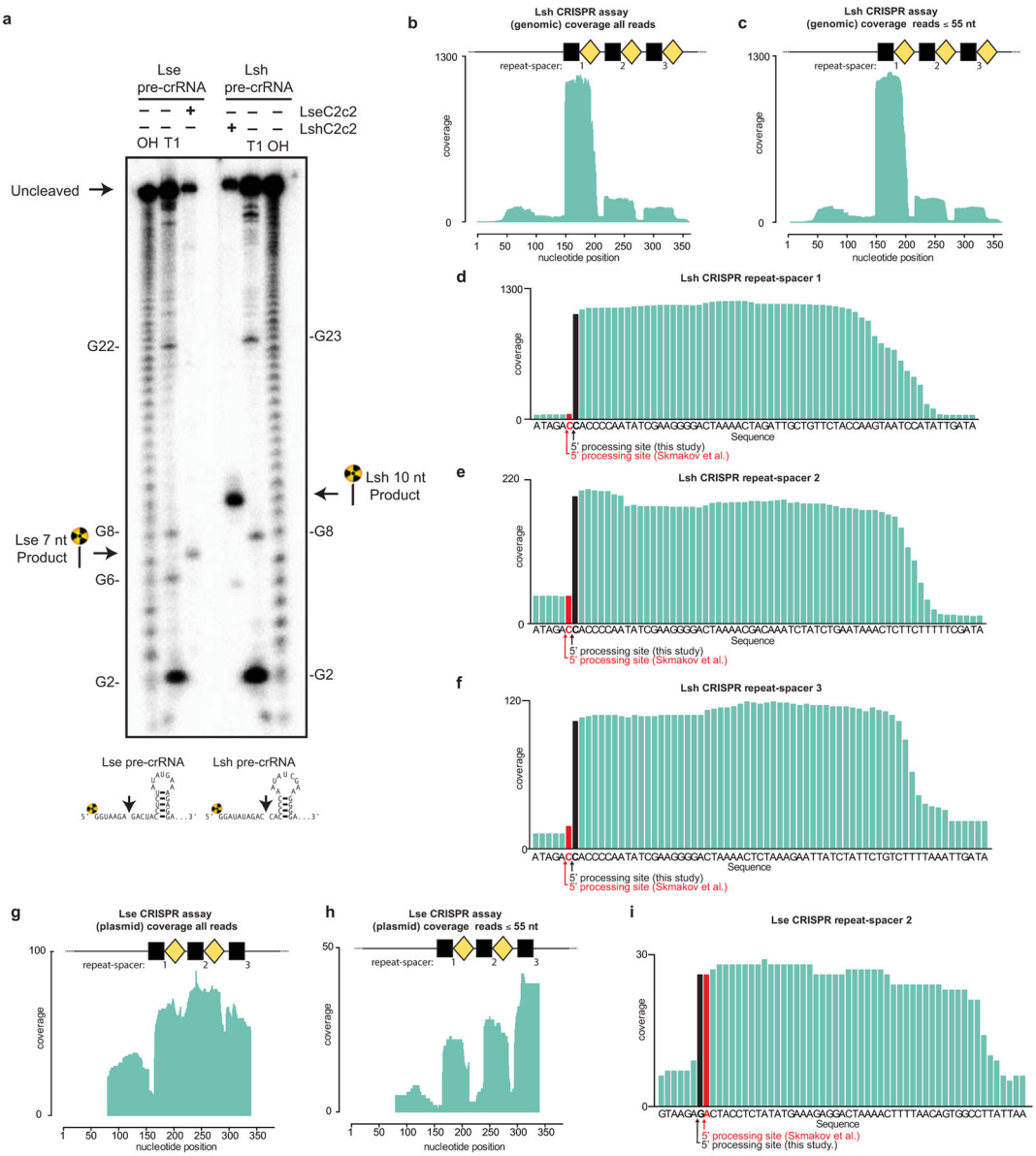

Extended Data Figure 3. Mapping of pre-crRNA processing by C2c2 *in vitro* and *in vivo*.

a, Cleavage site mapping of LseC2c2 and LshCc2c2 cleavage of a single cognate pre-crRNA array. OH: alkaline hydrolysis ladder; T1: T1 RNase hydrolysis ladder. Cleavage reactions were performed with 100 nM C2c2 and <1 nM pre-crRNA. **b–i,** Re-analysis of LshC2c2 (**b–f**) and LseC2c2 (**g–i)** CRISPR array RNA sequencing experiments from Shmakov *et al.*[10] (Fig. S7 and Fig. 5, respectively). All reads (**b,g**) and filtered reads (55 nt or less; as per original Shmakov *et al.* analysis; **c**,**h**) were stringently aligned to each CRISPR array using Bowtie2 (see Methods). Detailed views of individual CRISPR repeat-spacers are shown for Lsh (**d–f**) and Lse (**i**). Differences in 5′ end pre-crRNA processing are indicated by arrows below each sequence. BAM alignment files of our analysis are available in Supplementary Materials. This mapping clearly indicates that the 5′ ends of small RNA sequencing reads generated from Lsh pre-crRNAs map to a position 2 nts from the base of the predicted

hairpin, in agreement with our *in vitro* processing data (**a**). This pattern holds for all mature crRNAs detected from both native expression in *L. shahii* and heterologous expression in *E. coli* (data not shown, BAM file available in supplementary methods). Unfortunately, the LseC2c2 crRNA sequencing data (used in **g–i**) is less informative due to low read depth, and each aligned crRNA exhibits a slightly different 5′ end with little obvious uniformity. The mapping for one of the processed repeats (repeat-spacer 2; **i)** is in agreement with our data but only with low confidence due to the insufficient read depth.

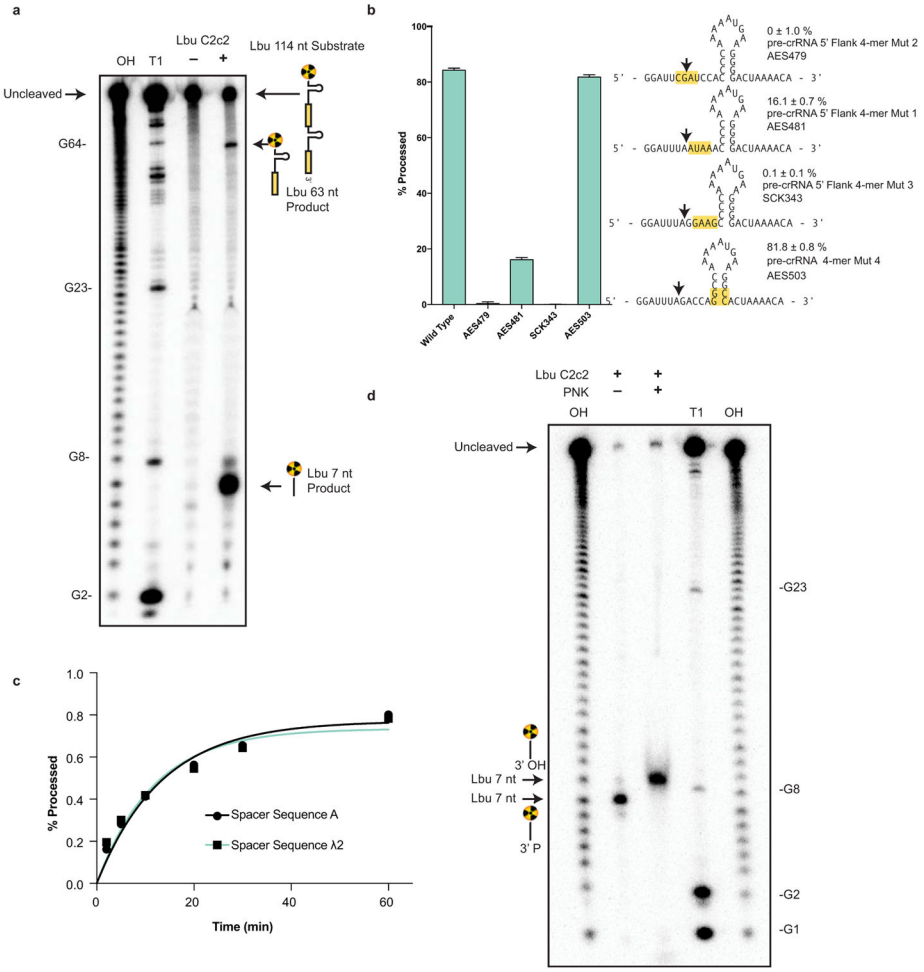

Extended Data Figure 4. Pre-crRNA processing by C2c2 is spacer-sequence independent, can occur on tandem crRNA arrays, is affected by mutations in the 5′ flanking region of the pre-crRNA and produces a 3′ phosphate product

a, Cleavage site mapping of LbuCc2c2 cleavage of a tandem pre-crRNA array. OH: alkaline hydrolysis ladder; T1: T1 RNase hydrolysis ladder. Cleavage reactions were performed with 100 nM LbuC2c2 and <1 nM pre-crRNA. A schematic of cleavage products is depicted on right, with arrows indicating the mapped C2c2 cleavage products. **b**, LbuC2c2 4-mer mutant pre-crRNA processing data demonstrating the importance of the 5′ single-stranded flanking region for efficient pre-crRNA processing. Percentage of pre-crRNA processing was measured after 60 min (mean ± s.d., n = 3). **c,** Representative LbuC2c2 pre-crRNA cleavage time-course demonstrating that similar rates of pre-crRNA processing occur independent of

crRNA spacer sequence pseudo-first-order rate constants (k_{obs}) (mean ± s.d.) are 0.07 ± 0.04 min^{-1} and 0.08 ± 0.04 min^{-1} for spacer A and spacer λ2, respectively. **d,** End group analysis of cleaved RNA by T4 polynucleotide kinase (PNK) treatment. Standard processing assay conditions were used to generate cleavage product, which was then incubated with PNK for 1 hr to remove any 2′, 3′-cyclic phosphates/3′ monophosphates. Retarded migration of band indicates removal of the charged, monophosphate from the 3′ end of radiolabeled 5′ product.

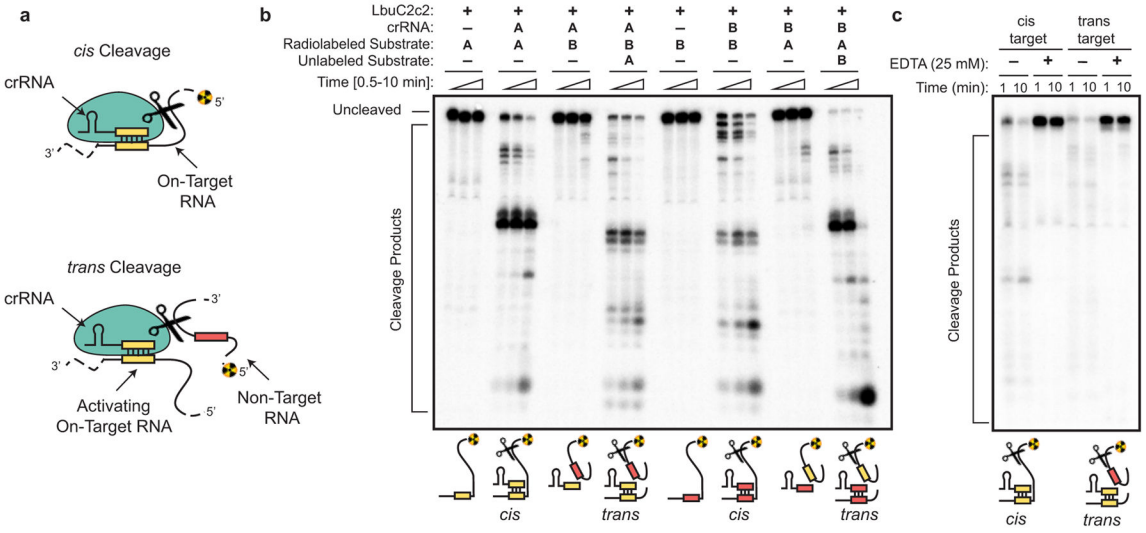

Extended Data Figure 5. LbuC2c2 catalyzes guide-dependent ssRNA degradation on *cis* and *trans* targets

a, Schematic of the two modes of C2c2, guide-dependent ssRNA degradation. **b,** Cleavage of two distinct radiolabeled ssRNA substrates, A and B, by LbuC2c2. Complexes of 100 nM C2c2 and 50 nM crRNA were pre-formed at 37 °C, and reaction was initiated upon addition of <1 nM 5′-labeled target RNA at 25°C. *Trans* cleavage reactions contained equimolar (<1 nM) concentrations of radiolabeled non-guide-complementary substrate, and unlabeled on-target ssRNA. For multiple ssRNA substrates, we observed that LbuC2c2 catalyzed efficient cleavage only when bound to the complementary crRNA, indicating that LbuC2c2:crRNA cleaves ssRNA in an RNA-guided fashion This activity is hereafter referred to as on-target or *cis*-target cleavage. LbuC2c2-mediated *cis* cleavage resulted in a laddering of multiple products, with cleavage preferentially occurring before uracil residues, analogous to LshC2c2[9]. We repeated non-target cleavage reactions in the presence of unlabeled, on-target (crRNA-complementary) ssRNA. In contrast to non-target cleavage experiments performed in *cis*, we observed rapid degradation of non-target RNA in *trans.* The similar RNA cleavage rates and near identical cleavage products observed for both *cis* on-target cleavage and *trans* non-target cleavage implicate the same nuclease center in both activities. **c,** LbuC2c2 loaded with crRNA targeting spacer A was tested for cleavage activity under both *cis* (target A labeled) and *trans* (target B labeled in the presence of unlabeled target A) cleavage conditions in the presence of 25 mM EDTA.

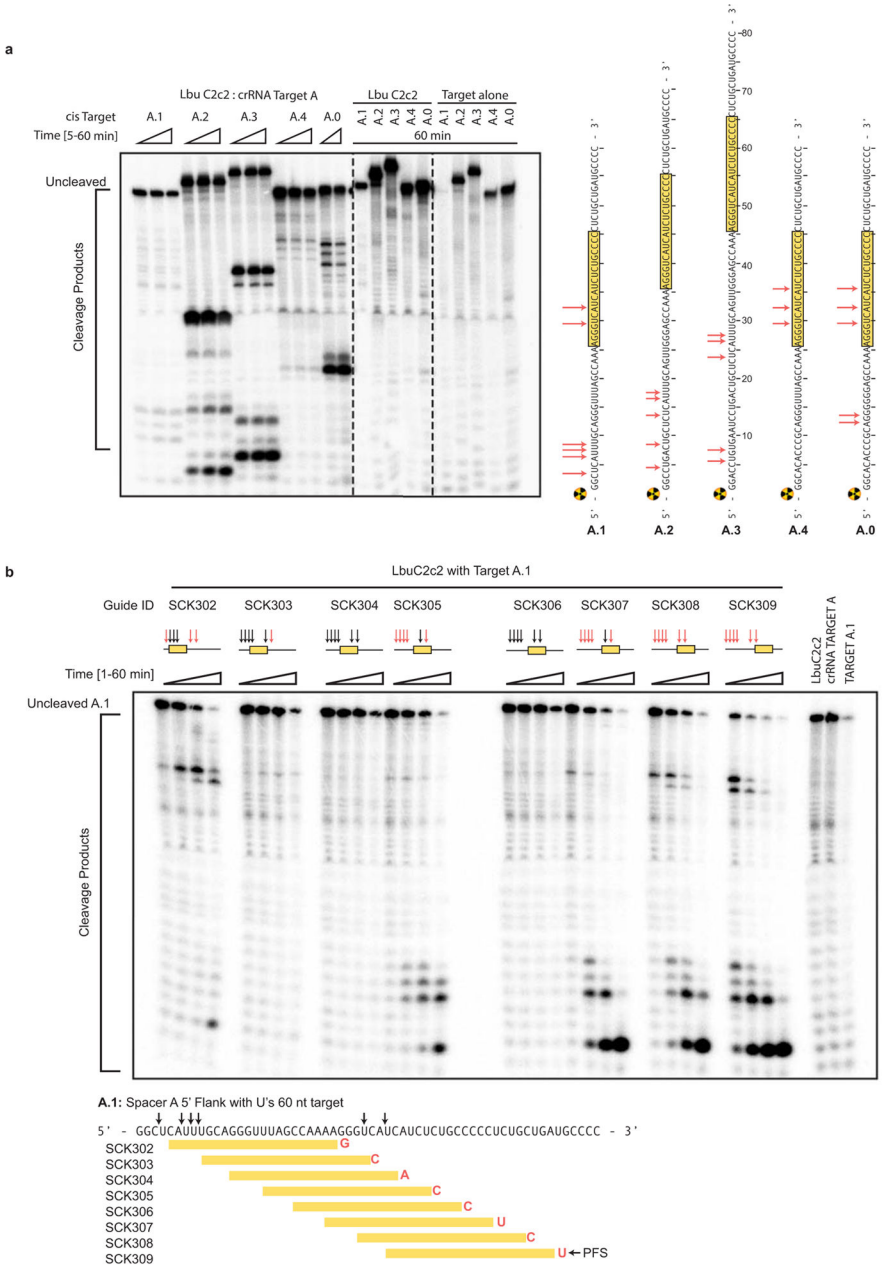

Extended Data Figure 6. LbuC2c2 ssRNA target cleavage site mapping

a, ssRNA target cleavage assay conducted per Methods demonstrating LbuC2c2-mediated '*cis*'-cleavage of several radiolabeled ssRNA substrates with identical spacer-complementary sequences but distinct 5′ flanking sequences of variable length and nucleotide composition. Sequences of ssRNA substrates are shown to the right with spacer-complementary sequences for crRNA-A highlighted in yellow. Arrows indicate detected cleavage sites. Gel was cropped for clarity. It should be noted that the pattern of cleavage products produced on different substrates (e.g. A.1 vs. A.2 vs. A.3) indicates that the cleavage site choice is primarily driven by a uracil preference and exhibits an apparent lack of exclusive cleavage mechanism within the crRNA-complementary target sequence, which

is in contrast to what is observed for other Class II CRISPR single effector complexes such as Cas9 and Cpf1[11,21]. Interestingly, the cleavage pattern observed for substrate A.0 hints at a secondary preference for polyG sequences. **b,** LbuC2c2 ssRNA target cleavage assay as per Methods, using a range of crRNAs that tile the length of the ssRNA target. The sequence of the ssRNA substrates used in this experiment is shown below the gel with spacer-complementary sequences for each crRNA highlighted in yellow. Arrows indicate predicted cleavage sites. Above each set of lanes, a small diagram indicates the location of the spacer sequence along the target (yellow box) and the cleavage products observed (red arrows) or absent (black arrows). Likewise, it should be noted that for every crRNA the cleavage product length distribution is very similar, again indicating an apparent lack of exclusive cleavage within the crRNA-bound sequence. The absence of a several cleavage products in a subset of the reactions might be explained by the presence of bound C2c2:crRNA on the ssRNA target, which could sterically occlude access to uracils by any *cis* (intramolecular) or *trans* (intermolecular) LbuC2c2 active sites. While proper analysis for protospacer flanking site (PFS) preference for LbuC2c2 is beyond the scope of this study, minimal impact of the 3′ flanking nucleotide was observed. Expected PFS base is noted in diagram next to each guide tested in red.

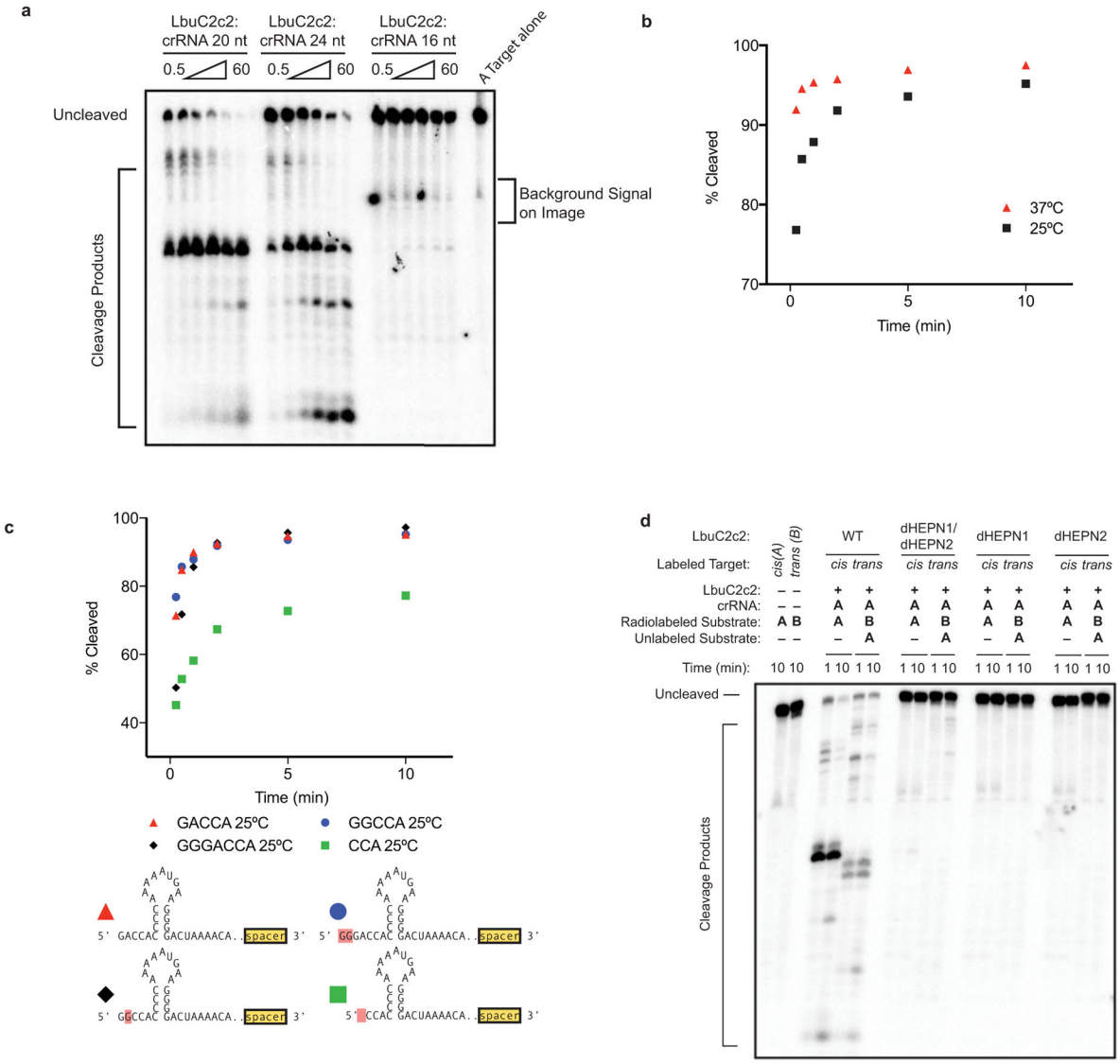

Extended Data Figure 7. Dependence of RNA targeting on crRNA variants, temperature and point mutations

a, LbuC2c2 ssRNA target cleavage assay carried out, as per Methods with crRNAs possessing 16-nt, 20-nt or 24-nt spacers. **b,** LbuC2c2 ssRNA target cleavage time-course carried out at either 25°C and 37°C as per methods. **c,** LbuC2c2 ssRNA target cleavage timecourse carried out as per Methods with crRNAs possessing different 5′-flanking nucleotide mutations. Mutations are highlighted in red. 1–2 nucleotide 5′ extensions negligibly impacted cleavage efficiencies. In contrast, shortening the flanking region to 3 nts slowed cleavage rates. **d** Impact of point mutations on ribonuclease activity of C2c2 in conserved residue mutants within HEPN motifs for ssRNA targeting.

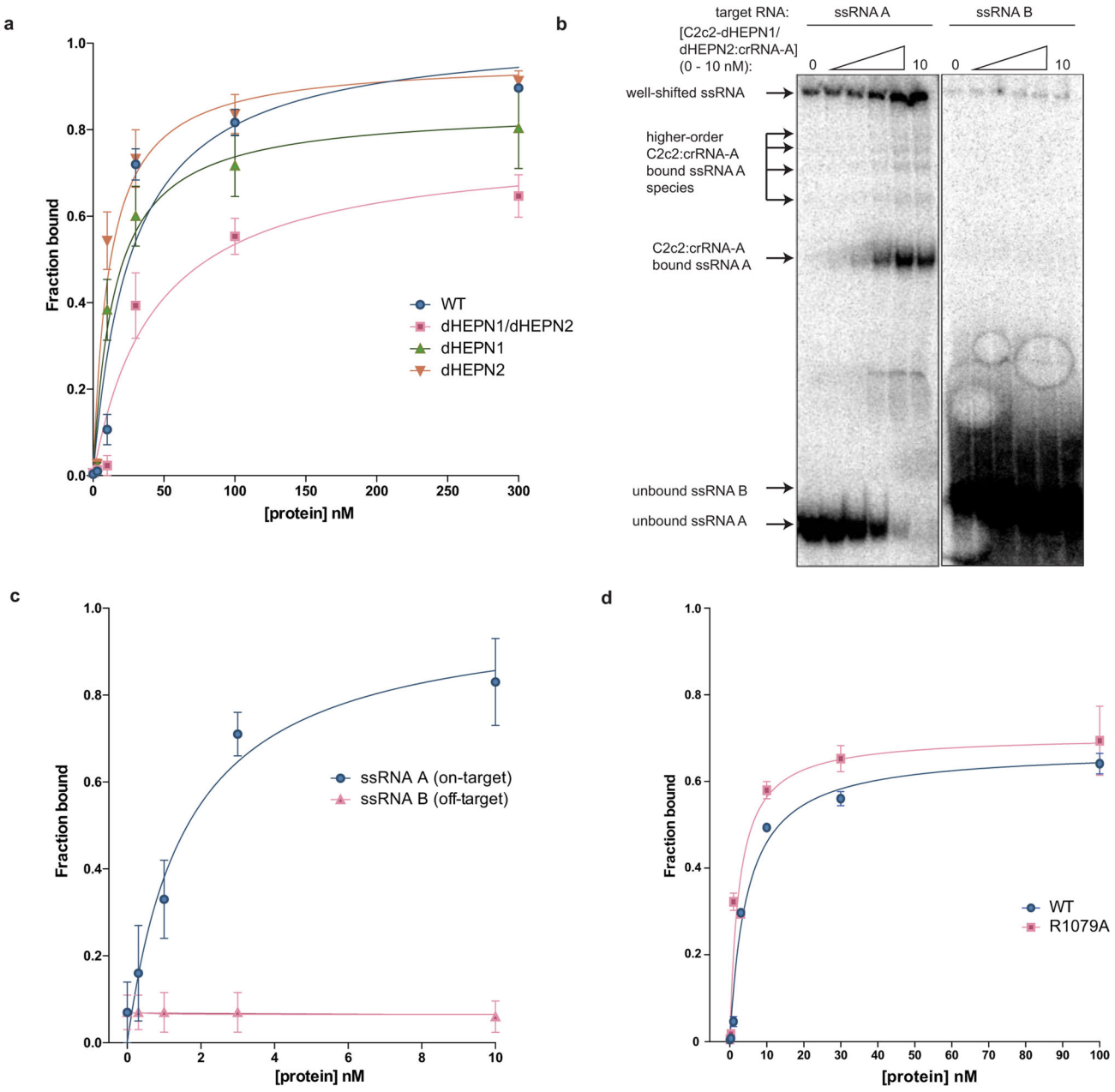

Extended Data Figure 8. Binding data for LbuC2c2 to mature crRNA and target ssRNA

a, Filter binding assays were conducted as described in the Methods to determine the binding affinity of mature crRNA-A_GG to LbuC2c2-WT, LbuC2c2-dHEPN1, LbuC2c2-dHEPN2, or LbuC2c2-dHEPN1/dHEPN2. The quantified data were fit to standard binding isotherms. Error bars represent the standard deviation from three independent experiments. Measured dissociation constants from three independent experiments (mean ± sd) were 27.1 ± 7.5 nM (LbuC2c2-WT), 15.2 ± 3.2 nM (LbuC2c2-dHEPN1), 11.5 ± 2.5 nM (LbuC2c2-dHEPN2), and 43.3 ± 11.5 nM (LbuC2c2- dHEPN1/dHEPN2). **b,** Representative electrophoretic mobility shift assay for binding reactions between LbuC2c2-dHEPN1/dHEPN2: crRNA-A_GG and either ‘on-target’ A ssRNA or ‘off-target’ B ssRNA, as

indicated. Three independent experiments were conducted as described in the Methods. The gel was cropped for clarity. **c,** Quantified binding data from (b) were fitted to standard binding isoforms. Error bars represent the standard deviation from three independent experiments. Measured dissociation constants from three independent experiments (mean ± sd) were 1.62 ± 0.43 nM for ssRNA A and N.D (≫10 nM) for ssRNA B. **d,** Filter binding assays were conducted as described in the Methods to determine the binding affinity of mature crRNA-A_GA to LbuC2c2-WT and LbuC2c2-R1079A. The quantified data were fit to standard binding isotherms. Error bars represent the standard deviation from three independent experiments. Measured dissociation constants from three independent experiments (mean ± sd) were 4.65 ± 0.6 nM (LbuC2c2-WT) and 2.52 ± 0.5 nM (LbuC2c2-R1079A). It is of note that these binding affinities differ from panel a. This difference is accounted for in a slight difference in the 5′ sequence of the guide with panel a guides beginning with a 5′-G**G**CCA… and panel d 5′-G**A**CCA. While the native sequence guide (5′-G**A**CCA) binds tighter to LbuC2c2, no difference is seen in the RNA targeting efficiencies of these guide variants (Extended Data Fig. 6c).

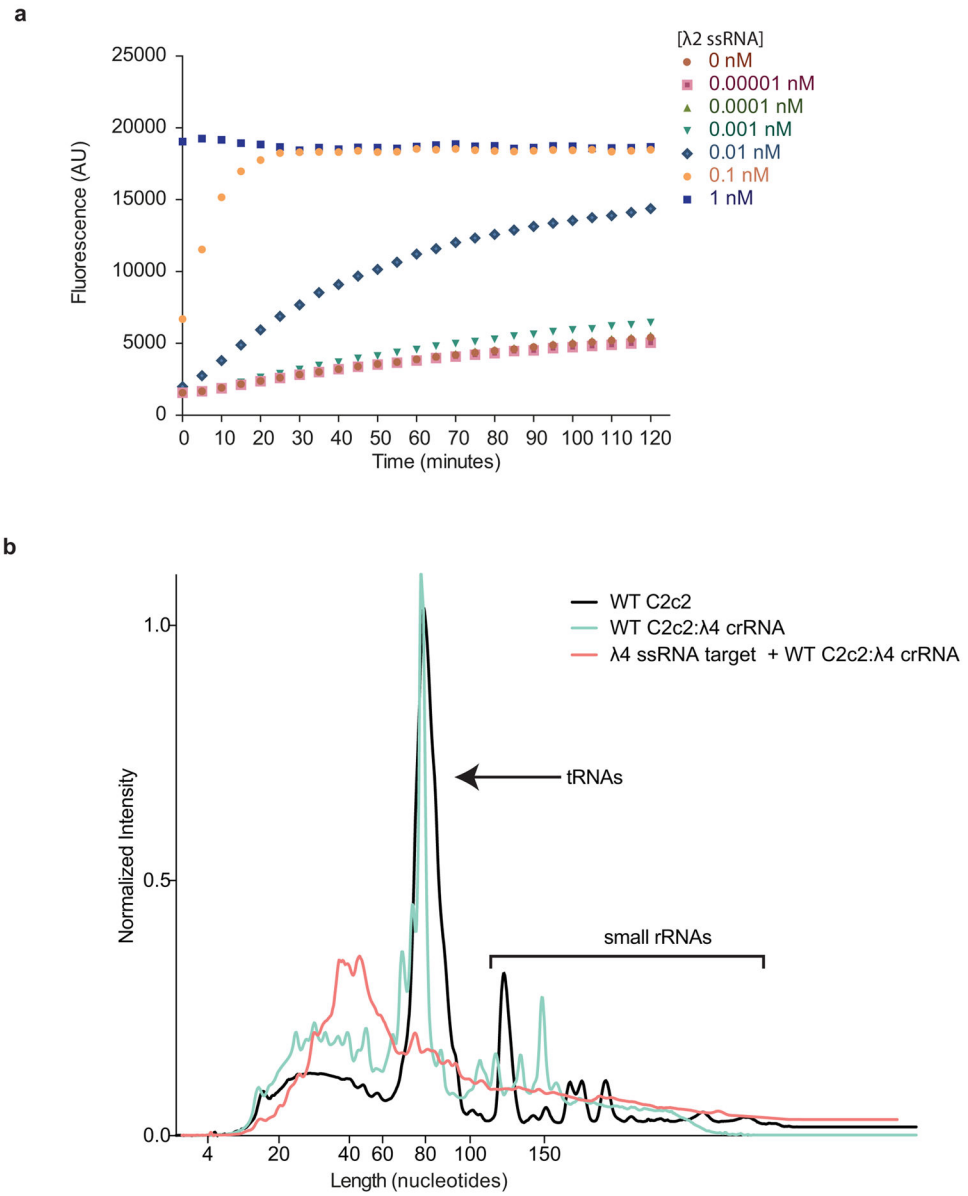

Extended Data Figure 9. RNase detection assay λ2-ssRNA time-course

a, LbuC2c2:crRNA-**λ**2 was incubated with RNAase-Alert substrate (Thermo-Fisher)) and 100 ng HeLa total RNA in the presence of increasing amounts of **λ**2 ssRNA (0–1 nM) for 120 min at 37°C. Fluorescence measurements were taken every 5 min. The 1 nM **λ**2 ssRNA reaction reached saturation before the first time point could be measured. Error bars represent the standard deviation from three independent experiments. **b,** LbuC2c2:crRNA-**λ**4 or apo LbuC2c2 was incubated in HeLa total RNA for 2 hours in the presence or absence of on-target activating **λ**4 ssRNA. Degradation of background small RNA was resolved on a small RNA chip in a Bioanalyzer 2100 as per Methods. Small differences are seen in the fragment profile of between apo LbuC2c2 and LbuC2c2:crRNA-**λ**4. In contrast, upon addition of the on-target ssRNA to the reaction, a drastic broadening and shifting of the

tRNA peak reveals extensive degradation of other structured and nonstructured RNA's present in the reaction upon activation of LbuC2c2 *trans* activity.

Extended Data Table 1

Oligonucleotides used in this study

Name	Sequence	Used in
Lbu_pre-crRNA_A_SCK314	5′-GGAUUUAGACCACCCCAAAAAUGAAGGGGACUAAAACAGGGGCAGAGAUGAUGACCCU-3′	Fig. 1c, 2a–c, 3a,c, ED3
Lse_pre-crRNA_B_AES484	5′-GGUAAGAGACUACCUCUAUAUGAAAGAGGACUAAAACCAAACAUGAUCUGGGUCAUC-3′	Fig. 1c, ED3
Lsh_pre-crRNA_A_SCK339	5′-GGAUUUAGACCACCCCAAUAUCGAAGGGGACUAAAACAGGGGCAGAGAUGAUGACCCU-3′	Fig. 1c. ED3
Lbu_pre-crRNA_invert_SCK321	5′-GGAUUUAGACCAGGGGAAGUAAAAACCCCACUAAAACAGGGGCAGAGAUGAUGACCCU-3′	Fig. 2a
Lbu_pre-crRNA_5stem_SCK331	5′-GGAUUUAGACCACCCCCAAAAAUGAAGGGGGACUAAAACAGGGGCAGAGAUGAUGACCCU-3′	Fig. 2a
Lbu_pre-crRNA_7bubble_SCK334	5′-GGAUUUAGACCACCCCAUGAAGGGGACUAAAACAGGGGCAGAGAUGAUGACCCU-3′	Fig. 2a
Lbu_pre-crRNA_5bubble_SCK335	5′-GGAUUUAGACCACCCCAUGAAGGGGACUAAAACAGGGGCAGAGAUGAUGACCCU-3′	Fig. 2a
Lbu_pre-crRNA_3stem_SCK342	5′-GGAUUUAGACCACCCCAAAAAUGAAGGGCACUAAAACAGGGGCAGAGAUGAUGACCCU-3′	Fig. 2a
Lbu_pre-cr_5′_mut1_AES497	5′-GGCGUUAGACCACCCCAAAAAUGAAGGGGACUAAAACAGGGGCAGAGAUGAUGACCCU-3′	Fig. 2b, ED4
Lbu_pre-cr_5′_mut2_AES496	5′-GGAGCUAGACCACCCCAAAAAUGAAGGGGACUAAAACAGGGGCAGAGAUGAUGACCCU-3′	Fig. 2b, ED4
Lbu_pre-cr_5′_mut3_AES495	5′-GGAUCCAGACCACCCCAAAAAUGAAGGGGACUAAAACAGGGGCAGAGAUGAUGACCCU-3′	Fig. 2b, ED4
Lbu_pre-cr_5′_mut4_AES477	5′-GGAUUCGGACCACCCCAAAAAUGAAGGGGACUAAAACAGGGGCAGAGAUGAUGACCCU-3′	Fig. 2b, ED4
Lbu_pre-cr_5′_mut5_AES482	5′-GGAUUUACCCCACCCCAAAAAUGAAGGGGACUAAAACAGGGGCAGAGAUGAUGACCCU-3′	Fig. 2b, ED4
Lbu_pre-cr_5′_mut6_AES478	5′-GGAUUUAAUCCACCCCAAAAAUGAAGGGGACUAAAACAGGGGCAGAGAUGAUGACCCU-3′	Fig. 2b, ED4
Lbu_pre-cr_5′_mut7_AES480	5′-GGAUUUAGAAAACCCCAAAAAUGAAGGGGACUAAAACAGGGGCAGAGAUGAUGACCCU-3′	Fig. 2b, ED4
Lbu_pre_cr_5′_mut8_AES498	5′-GGAUUUAGACCGCCCCAAAAAUGAAGGGGACUAAAACAGGGGCAGAGAUGAUGACCCU-3′	Fig. 2b, ED4
Lbu_pre_stem_mut1_AES502	5′-GGAUUUAGACCAGCCCAAAAAUGAAGGGCACUAAAACAGGGGCAGAGAUGAUGACCCU-3′	Fig. 2b, ED4
Lbu_pre_stem_mut2_AES501	5′-GGAUUUAGACCACCGCAAAAAUGAAGCGGACUAAAACAGGGGCAGAGAUGAUGACCCU-3′	Fig. 2b, ED4
Lbu_pre_stem_mut3_AES500	5′-GGAUUUAGACCACACCAAAAAUGAAGGUGACUAAAACAGGGGCAGAGAUGAUGACCCU-3′	Fig. 2b, ED4
Lbu_pre_stem_mut4_AES499	5′-GGAUUUAGACCACCACAAAAAUGAAGUGGACUAAAACAGGGGCAGAGAUGAUGACCCU-3′	Fig. 2b, ED4
Lbu_pre_stem_mut5_AES504	5′-GGAUUUAGACCACUCCAAAAAUGAAGGAGACUAAAACAGGGGCAGAGAUGAUGACCCU-3′	Fig. 2b, ED4
Lbu_pre_cr_3′_mut1_AES505	5′-GGAUUUAGACCACCCCAAAAAUGAAGGGGCAUAAAACAGGGGCAGAGAUGAUGACCCU-3′	Fig. 2b, ED4
Lbu_pre_cr_3′_mut2_AES506	5′-GGAUUUAGACCACCCCAAAAAUGAAGGGGACGCAAACAGGGGCAGAGAUGAUGACCCU-3′	Fig. 2b, ED4
Lbu_pre_cr_3′_mut3_AES507	5′-GGAUUUAGACCACCCCAAAAAUGAAGGGGACUAGCACAGGGGCAGAGAUGAUGACCCU-3′	Fig. 2b, ED4
Lbu_pre_cr_3′_mut4_AES508	5′-GGAUUUAGACCACCCCAAAAAUGAAGGGGACUAAAGUAGGGGCAGAGAUGAUGACCCU-3′	Fig. 2b, ED4
crLbu_A_GG_AES432	5′-GGCCACCCCAAAAAUGAAGGGGACUAAAACAGGGGCAGAGAUGAUGACCCU-3′	ED4–7
crLbu_B_AES451	5′-GGCCACCCCAAAAAUGAAGGGGACUAAAACACAAACAUGAUCUGGGUCAUC-3′	Fig. 3, ED 4
A.0_target_AES450	5′-GGCACACCCGCAGGGGGGAGCCAAAAGGGUCAUCAUCUCUGCCCCCACAGCAGAAGCCCC-3′	Fig. 3, ED4–7
B_target_AES452	5′-GGGAACCCCAAGGCCAACCGCGAGAAGAUGACCCAGAUCAUGUUUGAGACCUUCAACACCCC-3′	Fig. 3, ED4,6
crLbu_Lambda2_AES453	5′-GGCCACCCCAAAAAUGAAGGGGACUAAAACAGUGAUAAGUGGAAUGCCAUG-3′	Fig. 4b, ED 8
crLbu_Lambda3_MOC410	5′-GGCCACCCCAAAAAUGAAGGGGACUAAAACACUGGUGAACUUCCGAUAGUG-3′	Fig. 4b
crLbu_Lambda4_MOC411	5′-GGCCACCCCAAAAAUGAAGGGGACUAAAACACAGAUAUAGCCUGGUGGUUC-3′	Fig. 4b, ED 8
Lambda2_target_MOC28	5′-GGCUCAAUUUUGACAGCGGUCAUGGCAUUCCACUUAUCACUGGCAUCCUUCCACUC-3′	Fig. 4b, ED 8
Lambda3_target_MOC36	5′-GGAAAUCAUUCAACACCCGCACUAUCGGAAGUUCACCAGCCAGCCGCAGCACGUU-3′	Fig. 4b
Lambda4_target_MOC37	5′-GGCAAUAAAAAUGCGCCGCCUGAACCACCAGGCUAUAUCUGCCACUCAUUGUUGUGA-3′	Fig. 4b ED 8
crLbu_betaActin_1_AES451	5′-GGCCACCCCAAAAAUGAAGGGGACUAAAACACAAACAUGAUCUGGGUCAUC-3′	Fig. 4c
pre-crLbu_dimer_SCK324	5-′GGAUUUAGACCACCCCAAAAAUGAAGGGGACUAAAACAGGGGCAGAGAUGAUGACCCUAUUUAGACCACCCCAAAAAUGAAGGGGACUAAAACAGUGAUAAGUGGAAUGCCAUG-3′	Fig. 4d, ED3
crLbu_lambda2_SCK315	5′-GGAUUUAGACCACCCCAAAAAUGAAGGGGACUAAAACAGUGAUAAGUGGAAUGCCAUG-3′	ED3
Lbu_pre_cr_5′_4mer1_AES481	5′-GGAUUUAAUAAACCCCAAAAAUGAAGGGGACUAAAACAGGGGCAGAGAUGAUGACCCU-3′	ED3
Lbu_pre_cr_5′_4mer2_AES479	5′-GGAUUCGAUCCACCCCAAAAAUGAAGGGGACUAAAACAGGGGCAGAGAUGAUGACCCU-3′	ED3
Lbu_pre_cr_5′_4mer3_SCK343	5′-GGAUUUAGGAAGCCCCAAAAAUGAAGGGGACUAAAACAGGGGCAGAGAUGAUGACCCU-3′	ED3
Lbu_pre_cr_5′_4mer4_AES503	5′-GGAUUUAGACCAGGCCAAAAAUGAAGGCCACUAAAACAGGGGCAGAGAUGAUGACCCU-3′	ED3
crLbu_GuideWalk1_SCK302	5′-GGCCACCCCAAAAAUGAAGGGGACUAAAACAUUUUGGCUCCCCCCUGCAAAUGAG-3′	ED5
crLbu_GuideWalk2_SCK303	5′-GGCCACCCCAAAAAUGAAGGGGACUAAAACAACCCUUUGGCUCCCCCCUGCAAA-3′	ED5
crLbu_GuideWalk3_SCK304	5′-GGCCACCCCAAAAAUGAAGGGGACUAAAACAGAUGACCCUUUGGCUCCCCCCUG-3′	ED5
crLbu_GuideWalk4_SCK305	5′-GGCCACCCCAAAAAUGAAGGGGACUAAAACAAGAUGAUGACCCUUUGGCUCCCC-3′	ED5
crLbu_GuideWalk5_SCK306	5′-GGCCACCCCAAAAAUGAAGGGGACUAAAACAGCAGAGAUGAUGACCCUUUUGGCU-3′	ED5
crLbu_GuideWalk6_SCK307	5′-GGCCACCCCAAAAAUGAAGGGGACUAAAACAGGGGGCAGAGAUGAUGACCCUUUU-3′	ED5
crLbu_GuideWalk7_SCK308	5′-GGCCACCCCAAAAAUGAAGGGGACUAAAACACAGAGGGGGCAGAGAUGAUGACCC-3′	ED5
crLbu_GuideWalk8_SCK309	5′-GGCCACCCCAAAAAUGAAGGGGACUAAAACAUCAGCAGAGGGGGCAGAGAUGAUG-3′	ED5
A.1_target_U_MOC279	5′-GGCUCAUUUGCAGGGGGGAGCCAAAAGGGUCAUCAUCUCUGCCCCCUCUGCUGAUGCCCC-3′	ED5
A.2_target_70nt_AES447	5′-GGCCUGACUGCUCUCAUUUGCAGUUGGGAGCCAAAAGGGUCAUCAUCUCUGCCCCCUCUGCUGAUGCCCC-3′	ED5

Name	Sequence	Used in
A.3_target_80nt_AES448	5′-GGACCUGUGAAUCCUGACUGCUCUCAUUUGCAGUUGGGAGCCAAAAGGGUCAUCAUCUCUGCCCCCUCUGCUGAUGCCCC-3′	ED5
A.4_5′_ts_shift_AES449	5′-GGCACACCCGCAGGGUUUAGCCAAAAGGGUCAUCAUCUCUGCCCCCUCUGCUGAUGCCCC-3′	ED5
crLbu_A_16nt_trunc_SCK282	5′-GGCCACCCCAAAAAUGAAGGGGACUAAAACACAGAGAUGAUGACCCU-3′	ED6
crLbu_A_24nt_ext_SCK283	5′-GGCCACCCCAAAAAUGAAGGGGACUAAAACAAGAGGGGGCAGAGAUGAUGACCCU-3′	ED6
crLbu_A_mature_GA_SCK340	5′-GACCACCCCAAAAAUGAAGGGGACUAAAACAGGGGCAGAGAUGAUGACCCU-3′	ED6
crLbu_A_mature_GGGA_SCK341	5′-GGGACCACCCCAAAAAUGAAGGGGACUAAAACAGGGGCAGAGAUGAUGACCCU-3′	ED6
crLbu_A_mature_CCA_AES461	5′-CCACCCCAAAAAUGAAGGGGACUAAAACAGGGGCAGAGAUGAUGACCCU-3′	ED6
T7 Forward (DNA)	5′-TAATACGACTCACTATAGG-3′	N/A

Supplementary Material

Refer to Web version on PubMed Central for supplementary material.

Acknowledgments

We thank the QB3 MacroLab for assistance with cloning of C2c2 constructs; Nan Ma and Kaihong Zhou for technical assistance; S.N. Floor, S.C. Strutt, A.V. Wright, and M.L. Hochstrasser for critical reading of the manuscript, and members of the Doudna, Cate and Tjian laboratories for helpful discussions. S.C.K. acknowledges support from the National Science Foundation Graduate Research Fellowship Program; M.R.O. is a recipient of a C.J. Martin Overseas Early Career Fellowship from the National Health and Medical Research Council of Australia. This work was supported in part by a Frontiers Science award from the Paul Allen Institute to J.A.D., the National Science Foundation (MCB-1244557 to J.A.D.), and the California Institute for Regenerative Medicine (CIRM, RB4-06016 to R.T.). R.T. and J.A.D. are Investigators of the Howard Hughes Medical Institute. J.A.D. is a co-founder of Caribou Biosciences, Inc., Editas Medicine and Intellia Therapeutics. A.E.S., M.R.O., S.C.K., J.H.D.C., and J.A.D. have filed a patent application related to this work.

References

1. van der Oost J, Westra ER, Jackson RN, Wiedenheft B. Unravelling the structural and mechanistic basis of CRISPR-Cas systems. Nat Rev Microbiol. 2014; 12:479–492. [PubMed: 24909109]
2. Wright AV, Nunez JK, Doudna JA. Biology and Applications of CRISPR Systems: Harnessing Nature's Toolbox for Genome Engineering. Cell. 2016; 164:29–44. [PubMed: 26771484]
3. Brouns SJJ, et al. Small CRISPR RNAs Guide Antiviral Defense in Prokaryotes. Science. 2008; 321:960–964. [PubMed: 18703739]
4. Marraffini LA, Sontheimer EJ. CRISPR Interference Limits Horizontal Gene Transfer in Staphylococci by Targeting DNA. Science. 2008; 322:1843–1845. [PubMed: 19095942]
5. Garneau JE, et al. The CRISPR/Cas bacterial immune system cleaves bacteriophage and plasmid DNA. Nature. 2010; 468:67–71. [PubMed: 21048762]
6. Hale CR, et al. RNA-Guided RNA Cleavage by a CRISPR RNA-Cas Protein Complex. Cell. 2009; 139:945–956. [PubMed: 19945378]
7. Staals RHJ, et al. Structure and activity of the RNA-targeting Type III-B CRISPR-Cas complex of Thermus thermophilus. Molecular Cell. 2013; 52:135–145. [PubMed: 24119403]
8. Samai P, et al. Co-transcriptional DNA and RNA Cleavage during Type III CRISPR-Cas Immunity. Cell. 2015; 161:1164–1174. [PubMed: 25959775]
9. Abudayyeh OO, et al. C2c2 is a single-component programmable RNA-guided RNA-targeting CRISPR effector. Science. 2016; doi: 10.1126/science.aaf5573
10. Shmakov S, et al. Discovery and Functional Characterization of Diverse Class 2 CRISPR-Cas Systems. Molecular Cell. 2015; 60:385–397. [PubMed: 26593719]
11. Fonfara I, Richter H, Bratovič M, Le Rhun A, Charpentier E. The CRISPR-associated DNA-cleaving enzyme Cpf1 also processes precursor CRISPR RNA. Nature. 2016; 532:517–521. [PubMed: 27096362]
12. Li H. Structural Principles of CRISPR RNA Processing. Structure. 2015; 23:13–20. [PubMed: 25435327]

13. Charpentier E, Richter H, van der Oost J, White MF. Biogenesis pathways of RNA guides in archaeal and bacterial CRISPR-Cas adaptive immunity. FEMS Microbiology Reviews. 2015; 39:428–441. [PubMed: 25994611]
14. Hochstrasser ML, Doudna JA. Cutting it close: CRISPR-associated endoribonuclease structure and function. Trends in Biochemical Sciences. 2015; 40:58–66. [PubMed: 25468820]
15. Carte J, Wang R, Li H, Terns RM, Terns MP. Cas6 is an endoribonuclease that generates guide RNAs for invader defense in prokaryotes. Genes & Development. 2008; 22:3489–3496. [PubMed: 19141480]
16. Haurwitz RE, Jinek M, Wiedenheft B, Zhou K, Doudna JA. Sequence- and Structure- Specific RNA Processing by a CRISPR Endonuclease. Science. 2010; 329:1355–1358. [PubMed: 20829488]
17. Nam KH, et al. Cas5d Protein Processes Pre-crRNA and Assembles into a Cascade-like Interference Complex in Subtype I-C/Dvulg CRISPR-Cas System. 2012; 20:1574–1584.
18. Deltcheva E, et al. CRISPR RNA maturation by trans-encoded small RNA and host factor RNase III. Nature. 2011; 471:602–607. [PubMed: 21455174]
19. Fonfara I, et al. Phylogeny of Cas9 determines functional exchangeability of dual-RNA and Cas9 among orthologous type II CRISPR-Cas systems. Nucleic Acids Research. 2013; 42:2577–2590. [PubMed: 24270795]
20. Yang W. Nucleases: diversity of structure, function and mechanism. Quart Rev Biophys. 2011; 44:1–93.
21. Jinek M, et al. A Programmable Dual-RNA-Guided DNA Endonuclease in Adaptive Bacterial Immunity. Science. 2012; 337:816–821. [PubMed: 22745249]
22. Anantharaman V, Makarova KS, Burroughs AM, Koonin EV, Aravind L. Comprehensive analysis of the HEPN superfamily: identification of novel roles in intra-genomic conflicts, defense, pathogenesis and RNA processing. Biology Direct. 2013; 8:1–1. [PubMed: 23324625]
23. Sheppard NF, Glover CVC, Terns RM, Terns MP. The CRISPR-associated Csx1 protein of Pyrococcus furiosus is an adenosine-specific endoribonuclease. RNA. 2016; 22:216–224. [PubMed: 26647461]
24. Niewoehner O, Jinek M. Structural basis for the endoribonuclease activity of the type III-A CRISPR-associated protein Csm6. RNA. 2016; 22:318–329. [PubMed: 26763118]
25. Cordray MS, Richards-Kortum RR. Emerging nucleic acid-based tests for point-of-care detection of malaria. Am J Trop Med Hyg. 2012; 87:223–230. [PubMed: 22855751]
26. Rohrman BA, Leautaud V, Molyneux E, Richards-Kortum RR. A lateral flow assay for quantitative detection of amplified HIV-1 RNA. PLoS ONE. 2012; 7:e45611. [PubMed: 23029134]
27. Yan L, et al. Isothermal amplified detection of DNA and RNA. Mol Biosyst. 2014; 10:970–1003. [PubMed: 24643211]
28. McIlwain DR, et al. Caspase functions in cell death and disease. Cold Spring Harb Perspect Biol. 2013; 5:a008656. [PubMed: 23545416]
29. Choi UY, Kang JS, Hwang YS, Kim YJ. Oligoadenylate synthase-like (OASL) proteins: dual functions and associations with diseases. Exp Mol Med. 2015; 47:e144. [PubMed: 25744296]
30. Zhang J, Graham S, Tello A, Liu H, White MF. Multiple nucleic acid cleavage modes in divergent type III CRISPR systems. Nucleic Acids Research. 2016; 44:1789–1799. [PubMed: 26801642]
31. Stamatakis A. RAxML version 8: a tool for phylogenetic analysis and post-analysis of large phylogenies. Bioinformatics. 2014; 30:1312–1313. [PubMed: 24451623]
32. Katoh K, Standley DM. MAFFT Multiple Sequence Alignment Software Version 7: Improvements in Performance and Usability. Molecular Biology and Evolution. 2013; 30:772–780. [PubMed: 23329690]
33. Sternberg SH, Haurwitz RE, Doudna JA. Mechanism of substrate selection by a highly specific CRISPR endoribonuclease. RNA. 2012; 18:661–672. [PubMed: 22345129]
34. Langmead B, Salzberg SL. Fast gapped-read alignment with Bowtie 2. Nat Methods. 2012; 9:357–359. [PubMed: 22388286]

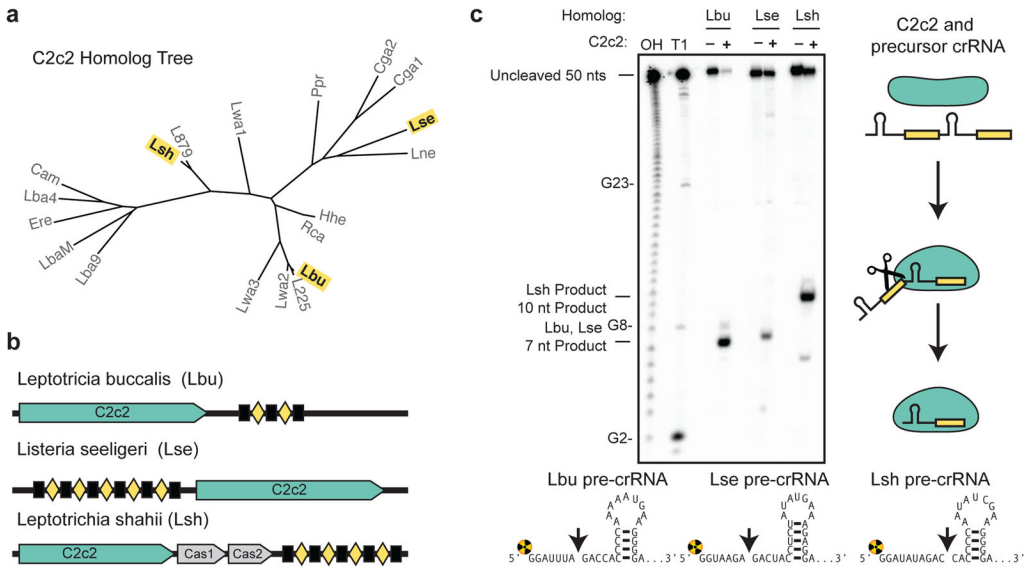

Figure 1. C2c2 proteins process precursor crRNA transcripts to generate mature crRNAs

a, Maximum-likelihood phylogenetic tree of C2c2 proteins. Homologs used in this study are highlighted in yellow. **b**, Diagram of the three Type VI CRISPR loci used in this study. Black rectangles denote repeat elements, yellow diamonds denote spacer sequences. Cas1 and Cas2 are only found in the genomic vicinity of LshC2c2. **c**, C2c2-mediated cleavage of pre-crRNA derived from the LbuC2c2, LseC2c2 and LshC2c2 CRISPR repeat loci. OH: alkaline hydrolysis ladder; T1: RNase T1 hydrolysis ladder; processing cleavage reactions were performed with 100 nM C2c2 and <1 nM pre-crRNA. Schematic of cleavage is depicted on right, and predicted pre-crRNA secondary structures are diagrammed below, with arrows indicating the mapped C2c2 cleavage sites.

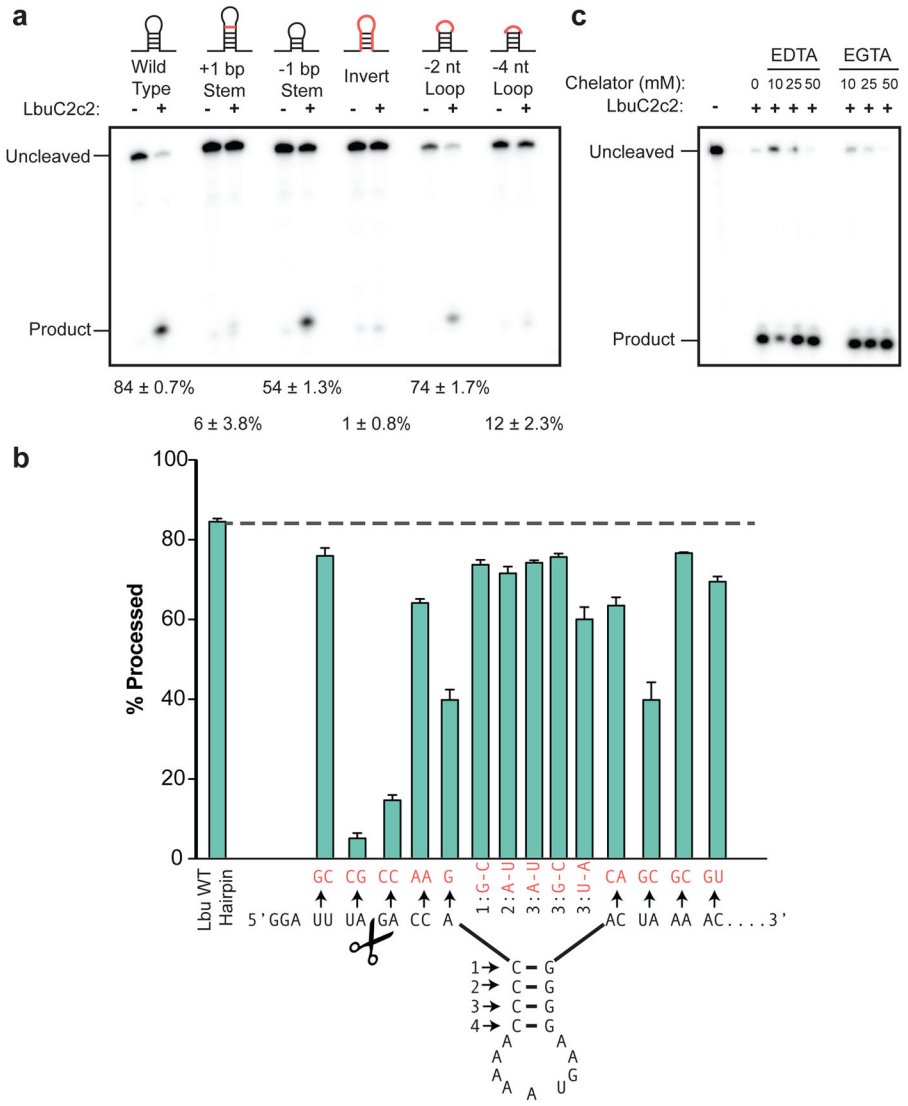

Figure 2. LbuC2c2 mediated crRNA biogenesis depends on both structure and sequence of CRISPR repeats

a, Representative cleavage assay by LbuC2c2 on pre-crRNAs containing structural mutations within the stem and loop regions of hairpin. Processed percentages listed below are quantified at 60 min (mean ± s.d., n = 3). **b**, Bar graph showing the dependence of pre-crRNA processing on the CRISPR repeat sequence. The wild-type repeat sequence is shown below with individual bars representing tandem nucleotide mutations as noted in red. The cleavage site is indicated by cartoon scissors. Percentage processed was measured after 60 min (mean ± s.d., n = 3). Diagrammed hairpins of tested mutants can be found in Extended Data Figs. 3–4 **c,** Divalent metal ion dependence of the crRNA processing reaction was tested by addition of 10–50 mM EDTA and EGTA to standard reaction conditions.

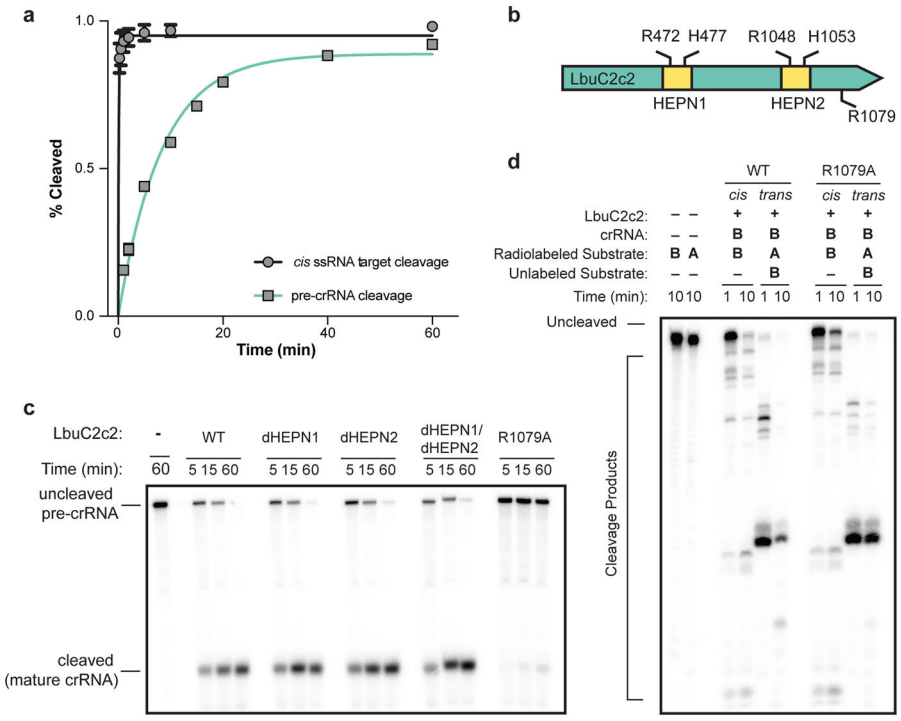

Figure 3. LbuC2c2 contains two distinct ribonuclease activities

a, Quantified time-course data of *cis* ssRNA target (black) and pre-crRNA (teal) cleavage by LbuC2c2 performed at 37°C. Exponential fits are shown as solid lines (n=3), and the calculated pseudo-first-order rate constants (k_{obs}) (mean ± s.d.) are 9.74 ± 1.15 min^{-1} and 0.12 ± 0.02 min^{-1} for *cis* ssRNA target and pre-crRNA cleavage, respectively. **b,** LbuC2c2 architecture depicting the location of HEPN motifs and processing deficient point mutant **c,d** Ribonuclease activity of LbuC2c2 mutants for pre-crRNA processing in **c** and ssRNA targeting in **d** and Extended Data Fig 6d.

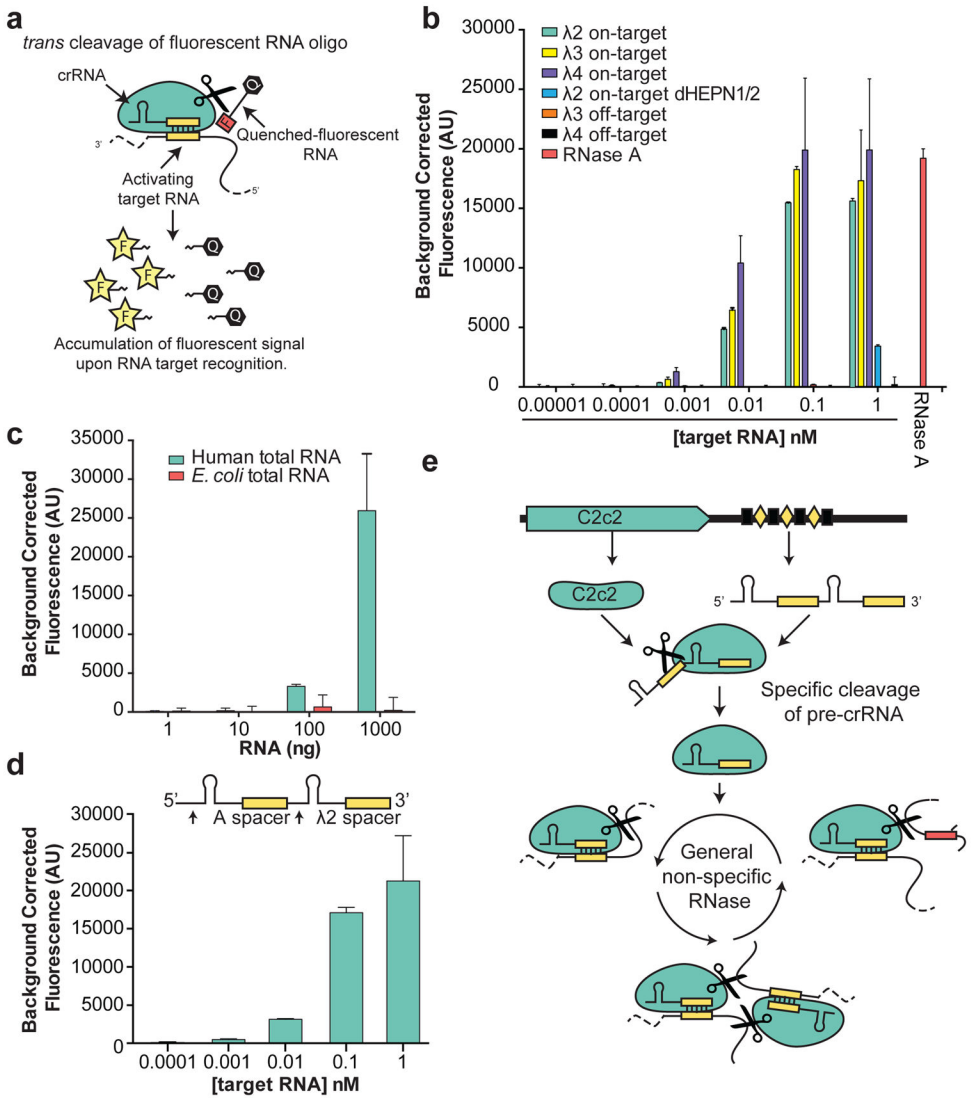

Figure 4. C2c2 provides sensitive detection of transcripts in complex mixtures

a, Illustration of LbuC2c2 RNA detection approach using a quenched fluorescent RNA reporter. **b**, Quantification of fluorescence signal generated by LbuC2c2 after 30 min for varying concentrations of target RNA in the presence of human total RNA. RNase A shown as positive RNA degradation control. (mean ± s.d., n = 3) **c**,. Quantification of fluorescence signal generated by LbuC2c2 loaded with a β-actin targeting crRNA after 3h for varying amounts of human total RNA or bacterial total RNA (as a β-actin null negative control). (mean ± s.d., n = 3) **d**, Tandem pre-crRNA processing also enables RNA detection. (mean ± s.d., n = 3) **e**, Model of the Type VI CRISPR pathway highlighting both of C2c2's ribonuclease activities.